Supplementary Material for

Sequence-dependent aggregation-prone conformations of islet amyloid polypeptide

Bumjoon Choi[1,#], Nam Hyeong Kim[2,#], Geun Young Jin[3], Yung Sam Kim[3], Yong Ho Kim[2,4,5,*], and Kilho Eom[1,*]

[1]Biomechanics Lab, College of Sport Science, Sungkyunkwan University (SKKU), Suwon 16419, Republic of Korea

[2]SKKU Advanced Institute of Nano Technology (SAINT), Sungkyunkwan University (SKKU), Suwon 16419, Republic of Korea

[3]Department of Chemistry, Ulsan National Institute of Science and Technology (UNIST), 50 UNIST-gil, Ulsan 44919, Republic of Korea

[4]Department of Nano Engineering, Sungkyunkwan University (SKKU), Suwon 16419, Republic of Korea

[5]Center for Neuroscience Imaging Research, Institute for Basic Science (IBS), Suwon 16419, Republic of Korea

[#]Theses authors contributed equally to this work

*Correspondence should be addressed to K.E. (E-mail: kilhoeom@skku.edu), or Y.H.K. (E-mail: yhkim94@skku.edu).

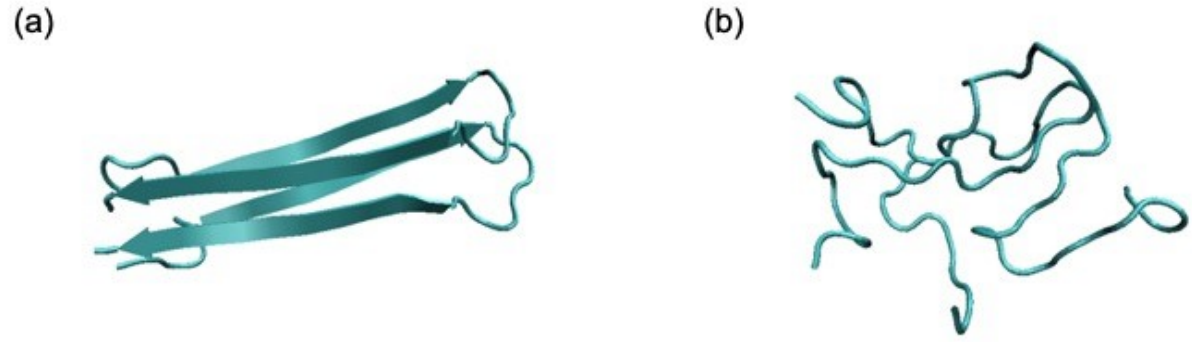

Fig. S1. (a) Dimeric structure extracted from the cross-β structure of hIAPP fibril derived from solid-state NMR before a brute force MD simulation was performed. (b) Random coil-like dimeric structure, obtained from 50 ns brute-force MD simulation, was used as an initial structure for REMD simulation.

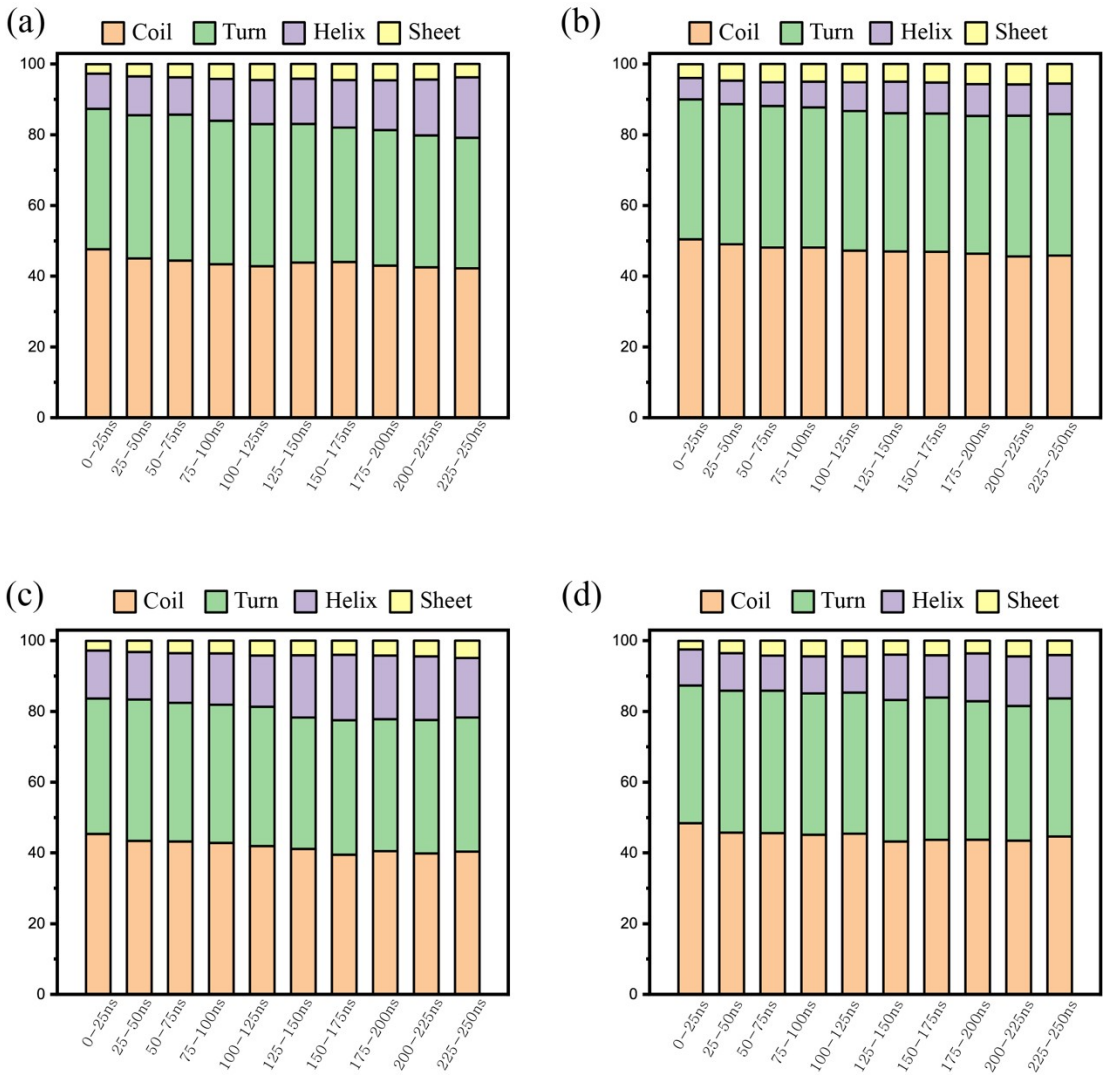

Fig. S2. Convergence tests based on block analysis for (a) hIAPP dimer, (b) rIAPP dimer, (c) hIAPP_S20G dimer, and (d) hIAPP_I26P dimer, respectively.

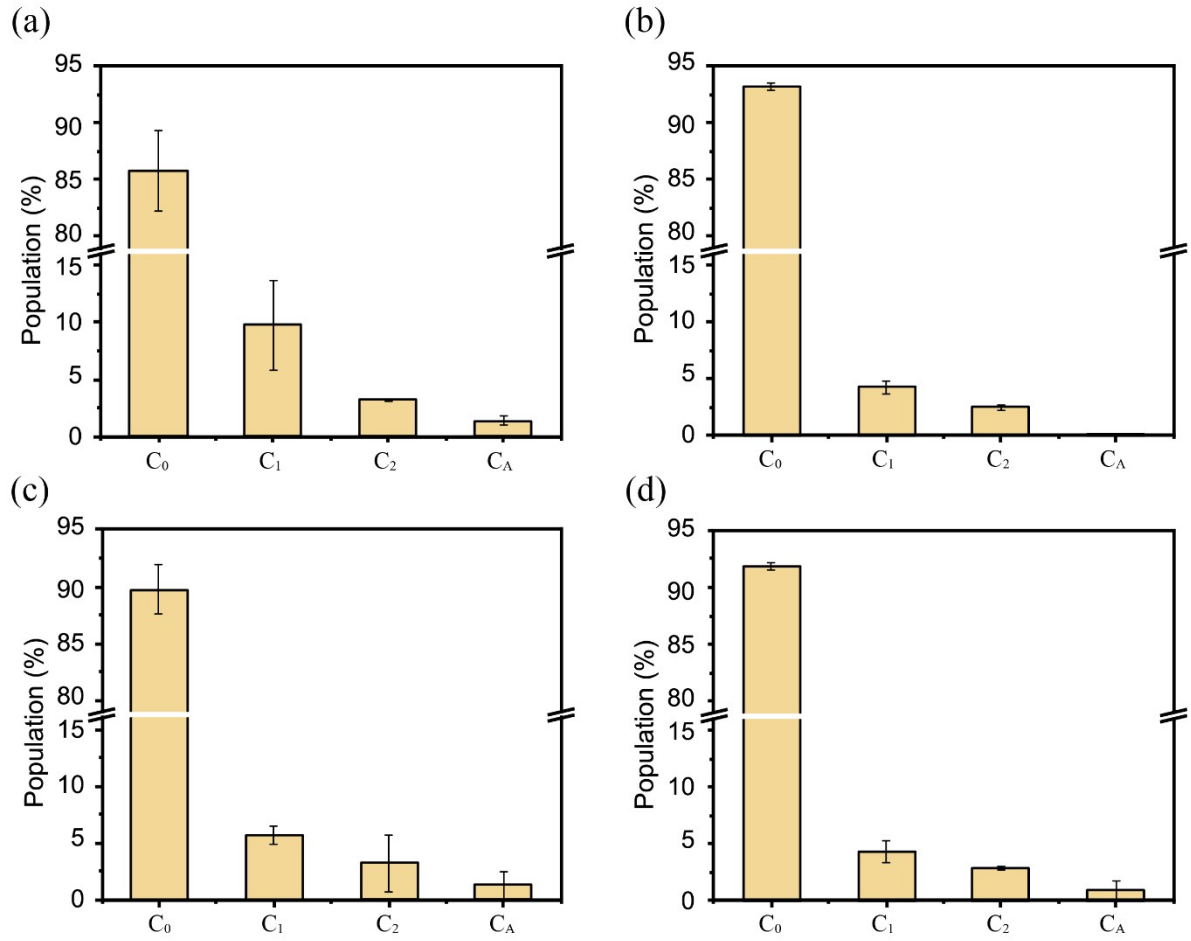

Fig. S3. Populations of aggregation-prone (C_A), β_1-forming (C_1), β_2-forming (C_2), and non-aggregation-prone (C_0) conformations for (a) hIAPP, (b) rIAPP, (c) hIAPP_S20G, and (d) hIAPP_I26P monomers. Here, error bar was calculated based on last 200ns trajectories that are divided into 2 blocks.

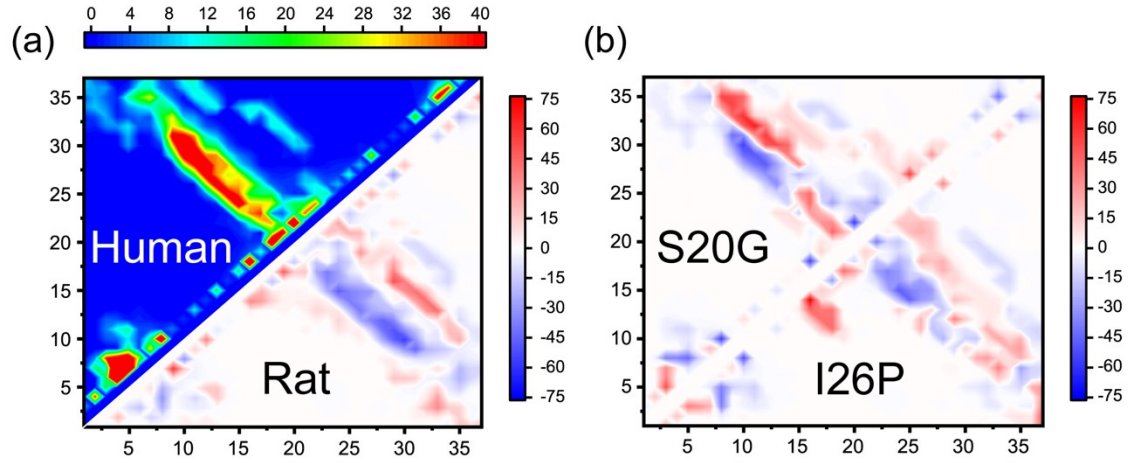

Fig. S4. (a) Contact map for aggregation-prone conformations (C_A) for hIAPP monomer (left upper panel), and the change of a contact map for C_A structures of rIAPP monomer with respect to hIAPP monomer (right lower panel). (b) The change of contact map for C_A structures of hIAPP_S20G monomer (left upper panel), or hIAPP_I26P monomer (right lower panel), with respect to hIAPP monomer.

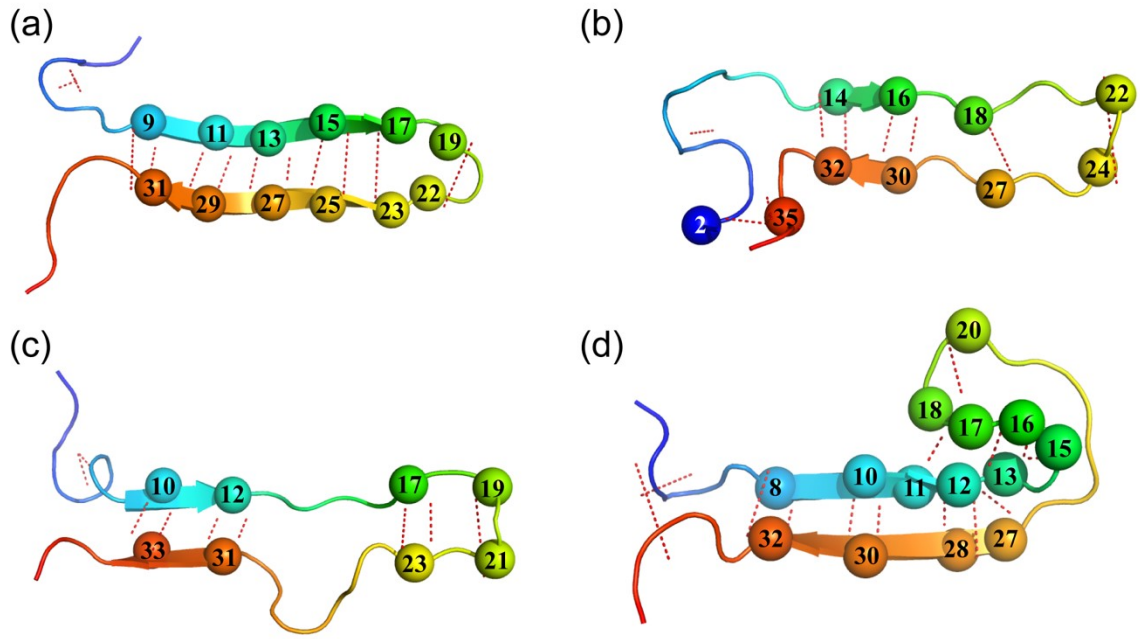

Fig. S5. Schematic representation of aggregation-prone conformations for (a) hIAPP monomer, (b) rIAPP monomer, (c) hIAPP_S20G monomer, and (d) hIAPP_I26P monomer, respectively. Here, red dashed lines between residues indicate the H-bonds.

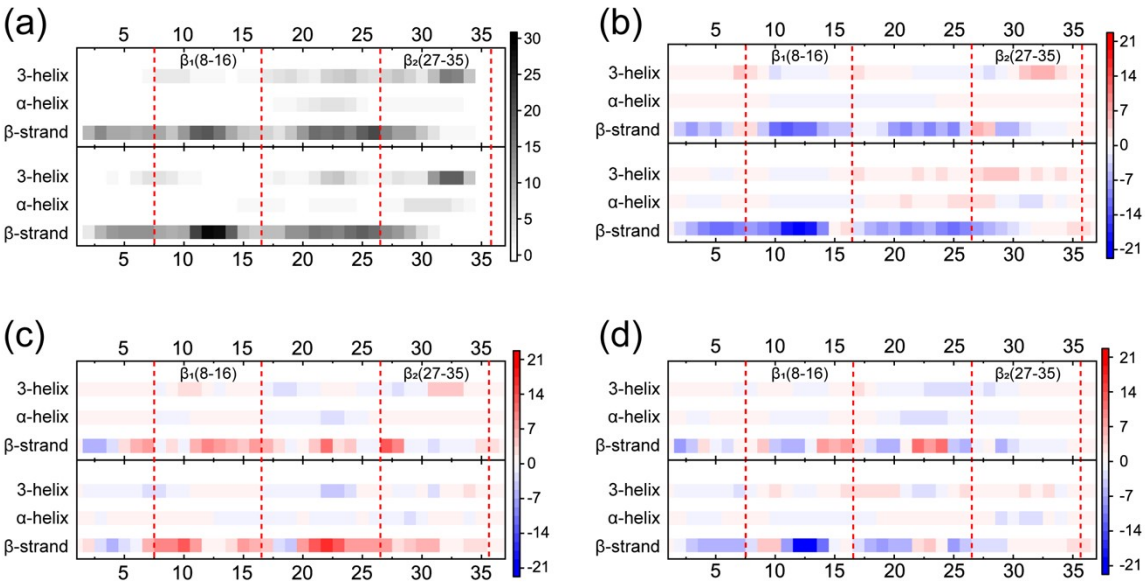

Fig. S6. Secondary structure analyses for four types of IAPP dimers. (a) Probabilities for each residue to form a secondary structure for hIAPP dimer. Changes of probabilities for each residue to construct a secondary structure for (b) rIAPP dimer, (c) hIAPP_S20G dimer, or (d) hIAPP_I26P dimer with respect to the probabilities for hIAPP dimer.

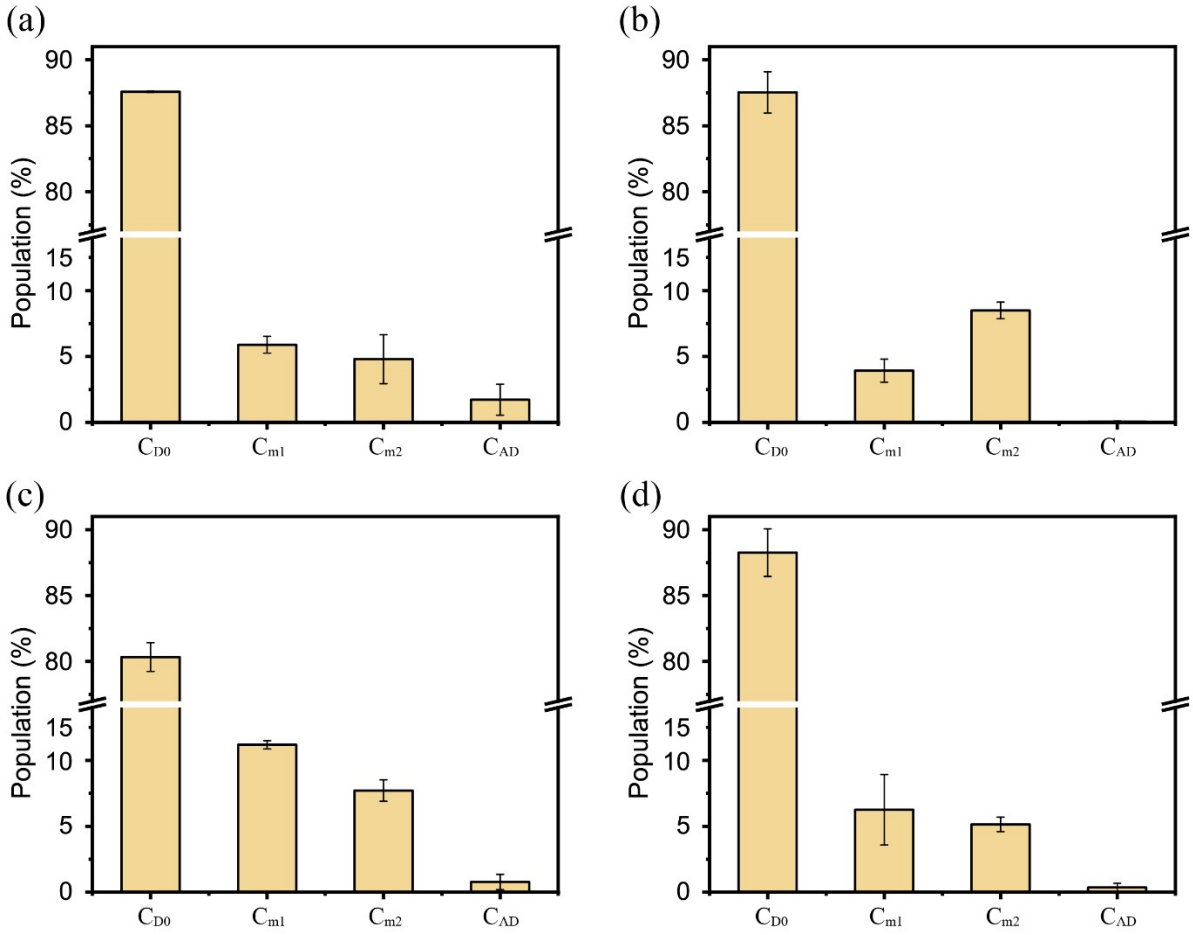

Fig. S7. Populations of aggregation-prone (C_A), monomer 1-ordered (C_{m1}), monomer 2-ordered (C_{m2}), and non-aggregation-prone (C_{D0}) conformations for (a) hIAPP dimer, (b) rIAPP dimer, (c) hIAPP_S20G dimer, and (d) hIAPP_I26P dimer. Here, the error bar was calculated based on last 200ns trajectories that are divided into 2 blocks.

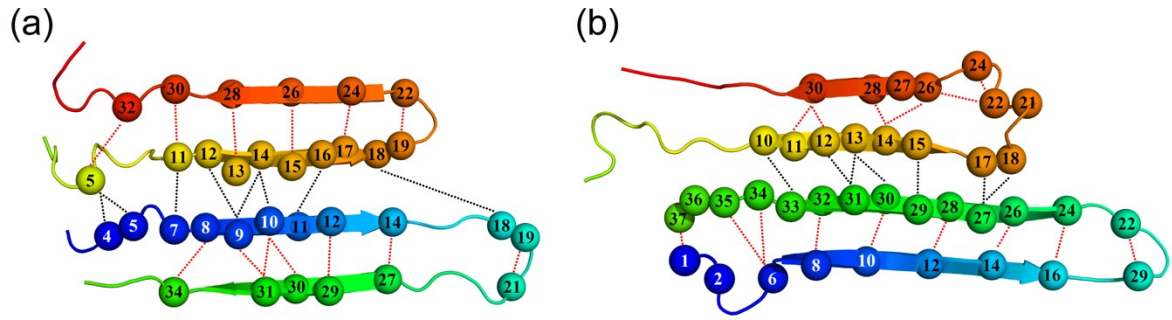

Fig. S8. Schematic representation of C_A structures for (a) hIAPP dimer, and (b) hIAPP_S20G dimer.

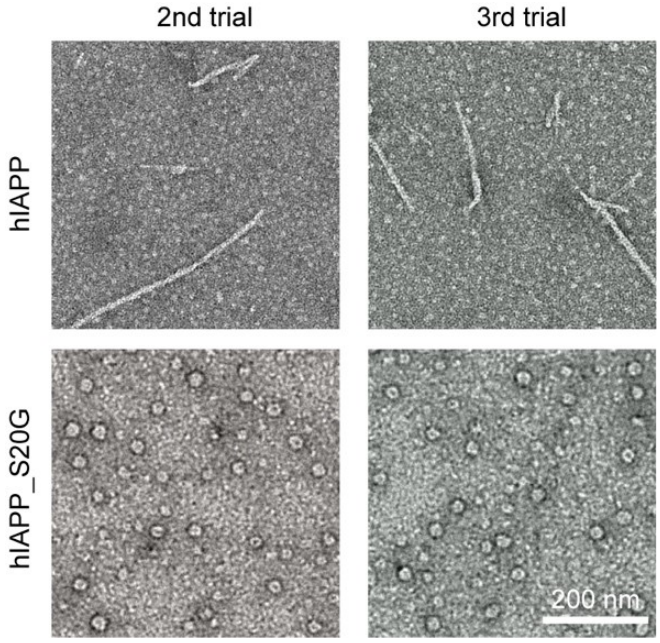

Fig. S9. TEM images of different samples for hIAPP and hIAPP_S20G aggregates. These TEM images confirm the reproducibility of our experimental finding that hIAPP aggregation leads to the formation of amyloid fibril, while hIAPP_S20G aggregation results in the barrel-like oligomer structures.

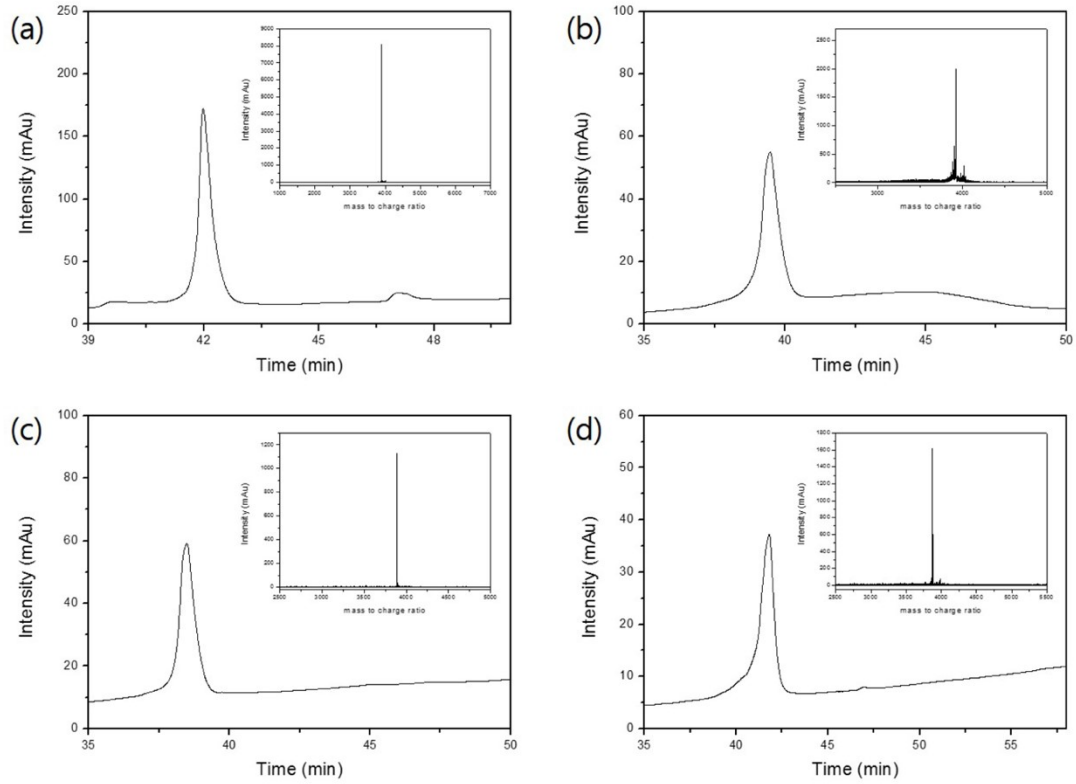

Fig. S10. Matrix assisted laser desorption/ionization-time of flight (MALDI-TOF) spectra for (a) hIAPP, (b) rIAPP, (c) hIAPP_S20G, and (d) hIAPP_I26P

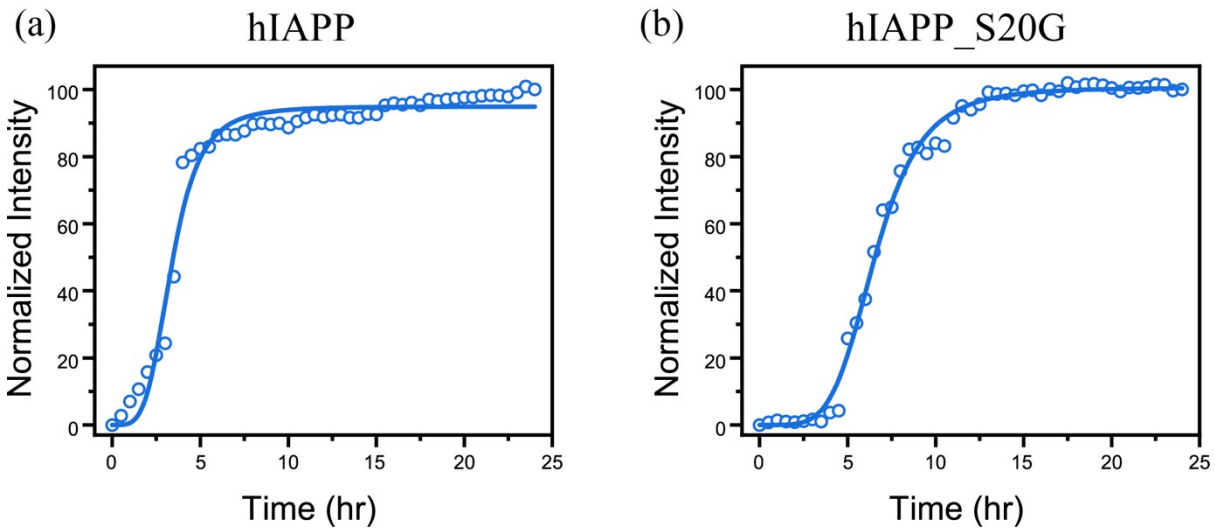

Fig. S11. ThT fluorescence spectra as a function of incubation time for (a) hIAPP aggregation, and (b) hIAPP_S20G aggregation.